

Intersection Crash Frequency Analysis Considering Visual Environment Features Using Random Parameter Negative Binomial-Lindley Model

Lei Han¹ , Mohamed Abdel-Aty¹ , Yang-Jun Joo¹ , Shaoyan Zhai¹, and Dongdong Wang¹ 

Abstract

Existing intersection crash analysis studies primarily consider macro infrastructure and traffic conditions. However, drivers' micro-level visual perception of the surrounding environment also affects their driving behaviors and, thus, safety, and this has not been fully investigated yet for intersection crash modeling. Leveraging recent image semantic segmentation techniques, this study extracts six types of visual object from Google Street View (GSV) images: sky, road, buildings, vegetation, vehicles, and walk area. Their pixel proportions were then aggregated as the drivers' visual environment features. These features, along with geometric design, traffic, and socioeconomic features, were combined into a random parameter negative binomial-Lindley (RPNB-L) model to analyze their impact on intersection crashes. Data from 501 Florida, U.S., signalized intersections were used for the empirical study. Results show that: 1) Compared with conventional models, the RPNB-L model achieves a superior fit by employing a mixed distribution to capture the heterogeneous effects of features; 2) Incorporating drivers' visual environment features enhances model fit as evidenced by lower deviance information criterion, mean absolute error, mean squared error, and a higher McFadden's pseudo R^2 ; 3) For total crashes, intersections near more underserved communities suffer more crashes. Two visual environment features (i.e., buildings and vegetation) are significantly negatively correlated with crash frequency; and 4) For different crash types, the contributing factors differ. A high proportion of buildings and vegetation at intersections are correlated with a reduction in rear-end, sideswipe, and severe crashes. However, the proportions of road and vehicle increase visual complexity, thus being significantly positively correlated with the frequency of rear-end crashes and crashes involving vulnerable road users.

Keywords

data and data science, statistical methods, safety, safety performance and analysis, crash frequency

Intersections are considered crash-prone locations because of the complex vehicle movements, multimodal interaction, and conflicts from different approaches. According to the Federal Highway Administration, approximately one-quarter of traffic fatalities and about one-half of all traffic injuries in the U.S. each year are associated with intersections (1). In 2021, there were 11,799 traffic fatalities at intersections, causing a huge loss of people's lives and property (2). To improve intersection traffic safety, extensive efforts have been made in intersection crash frequency modeling and safety evaluation (3–6). By establishing the relationship between intersection crash frequency and potential contributing factors, these studies can identify critical factors and

hotspots, thereby helping traffic managers implement targeted countermeasures and policies to prevent crashes (7, 8).

Among existing studies, four types of feature have been mainly evaluated for their effects on intersection crash frequency: geometric design, roadway traffic, signal control, and surrounding socioeconomic characteristics.

¹Department of Civil, Environmental, and Construction Engineering, University of Central Florida, Orlando, FL

Corresponding Author:
Lei Han, lei.han@ucf.edu

- 1) Geometric design characteristics: factors such as the number of lanes, skewed lanes, and median width were found to be positively correlated with intersection crash frequency (6, 9, 10). Conversely, the presence of shared or exclusive right-turn lanes could decrease the crash frequency (3, 11).
- 2) Roadway traffic features: most traffic-volume-related variables were found to have significant positive effects on crash frequency, including total entering annual average daily traffic (AADT), the log of AADT of major/minor roadways, and right- or left-turn AADT (4, 10, 12–16).
- 3) Signal control settings: adaptive signal control has been found to have lower crashes than fixed-time signal control (5, 16). The left-turn protection signal could significantly improve overall traffic safety (11, 15). The phase number was positively associated with the crash frequency (3, 17).
- 4) Socioeconomic features: the population, the number of nearby bus stops, and commercial land use were found to have significant positive correlation with the intersection crash frequency (15, 18, 19). Areas with high income and education levels tend to have fewer intersection crashes and severe crashes (15, 20).

However, the existing features only reflect the static infrastructure and traffic conditions, and ignore the drivers' visual perception of the surrounding driving environment. During driving on roads, the visual environment could significantly influence drivers' driving behaviors and, thus, safety (21–23). Recent advancements in computer vision have enabled researchers to extract visual environment features from street view images and dash camera footages. For instance, Kwon and Cho extracted building environment features from street view images to investigate factors influencing the subjective crash risk of children (24). Cai et al. proposed several visual measures from Google Street View (GSV) images to reflect drivers' visual environment and estimated its impact on urban arterial speeding crashes (25). Abdel-Aty et al. extracted semantic features from drivers' dash cameras and explored their relationships with speeding behaviors, showing that drivers are more likely to speed in an open area without trees and buildings (21). Yue investigated the influence of streetscape environment characteristics on pedestrian crashes at intersections using street view images (26). The findings from these studies highlight the importance of incorporating the driver's visual environment's features into crash analysis and traffic safety policymaking. However, existing studies tend to focus primarily on road segments or specific crash type, lacking a comprehensive evaluation of the relationships between complex visual features and intersection crashes.

In addition, while recent studies have employed machine learning models (e.g., XGBoost) for accurate crash predictions, these methods suffer limitations in statistical interpretability and overlook the heterogeneous effects of visual features.

To bridge this gap, this study aims to extract drivers' visual environment features at intersections and explore their impact on the crash frequency at signalized intersections. The main contributions of this study are:

- 1) Extract and integrate the drivers' visual environment features from GSV images into intersection crash frequency modeling.
- 2) Develop a random parameter negative binomial-Lindley (RPNB-L) model to capture the heterogeneous impact of visual environment features on intersection crashes.
- 3) Investigate the diverse impact of drivers' visual environment features on different crash scenarios (e.g., rear-end, sideswipe, severe, and vulnerable road user crashes).

The next section presents the data preparation, followed by a section showing the details of the proposed methodology and another illustrating the experiment results. The conclusions of this study are presented in the final section.

Data Preparation

In this study, a total of 501 signalized intersections in Hillsborough County, Florida, were selected because of the availability of open-source road design and traffic data (as shown in Figure 1). For each intersection, there is one target variable, that is, crash frequency data, and five major categories of explanatory variable: 1) traffic flow, 2) intersection geometric design, 3) socioeconomic characteristics, 4) road context classifications, and 5) GSV images data.

Crash Data

The crash data, covering the period from 2021 to 2023, were obtained from the Signal Four Analytics (S4A) system of Florida Department of Transportation (FDOT) (<https://signal4analytics.com>). This online platform includes all crash records in Florida. For each crash, it has the crash time, location, type, severity, number of involved vehicles, and other detailed information. According to the S4A system, crashes that occur within 250 ft of the stop line are defined as "intersection-related crashes." Thus, within-intersection and intersection-related crashes were identified and used in the analysis. Among these,

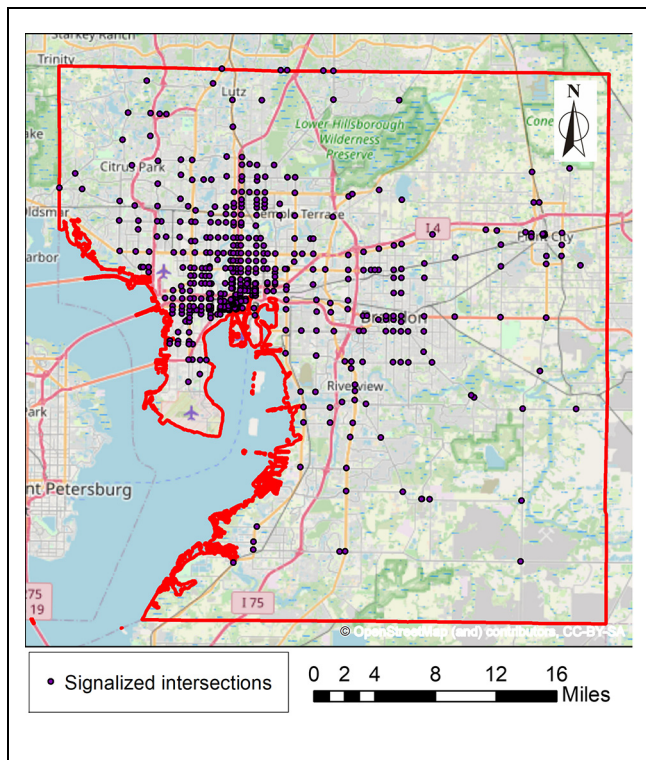


Figure 1. Signalized intersections in Hillsborough County, FL.

four specific types of crash were identified for further analysis: rear-end, sideswipe, severe (including fatality and serious injury crashes), and vulnerable road user crashes (including pedestrian and bicycle crashes).

Traffic Flow Data

Traffic flow data include the traffic volume at each intersection. Existing studies show that this can be represented by the AADT over 3 years (2021–2023), including AADT and truck AADT from major roads and minor roads (6, 11, 15). These data were collected from the open-source FDOT Roadway Characteristics Inventory (RCI) (<https://www.fdot.gov/statistics/gis/default.shtm>).

Intersection Geometric Design Data

The intersection geometric design features can also be obtained from the FDOT RCI system. For example, the posted speed limit is available for each roadway, allowing this information to be matched with the major and minor roadways at the intersections. Finally, a total of 26 geometric design features, which are believed to be related to the crash occurrence, were extracted (as shown in Table 1) (4, 27, 28).

Socioeconomic Data

Socioeconomic data reflect the features of the regional economy and population surrounding the intersections. To extract such features, census-tract-level data were used from the United States Department of Transportation (U.S. DOT) Equitable Transportation Community (ETC) Project (<https://www.transportation.gov/priorities/equity/justice40/etc-explorer>). This project collected five types of indicator (e.g., transportation insecurity, environmental burden, social vulnerability) to estimate the disadvantage level of communities. Multiple socioeconomic features were derived from such ETC datasets. Since a single intersection may be near multiple census tracts, a 0.5 mi buffer was created around each intersection (as illustrated in Figure 2) (29, 30). Socioeconomic features from the census tracts that spatially overlapped with this buffer were aggregated for the intersections. A weighted average was utilized, as suggested by existing studies (15). For example, the average population variable E_i for the intersection buffer i can be calculated:

$$E_i = \sum_j \frac{A_{j,i}}{A_j} * E_j \quad (1)$$

where

E_j = the population of census tract j ,

$A_{j,i}$ = the area of census tract j within buffer i , and

A_j = the area of the census tract j .

Meanwhile, several census tracts were identified as “underserved”—those with high poverty, low educational attainment, insufficient local jobs, and low homeownership. Previous research shows that underserved census tracts are more prone to experiencing traffic crashes (20, 31). Therefore, the count of underserved census tracts (Num_Underserved) within the intersection buffer was also used to reflect the overall socioeconomic vulnerability surrounding the intersections.

Road Context Classifications

Considering that traffic patterns vary significantly between urban, suburban, and rural areas, the context classifications of roadways were obtained from the Land Use and Infrastructure Plan of Hillsborough County (<https://hcfl.gov/government/county-projects/land-use-and-infrastructure-studies/land-use-and-infrastructure-other-publications>). Based on the surrounding land use, roadways were divided into six categories (e.g., C1 and C2 for natural and rural areas, C3C for suburban commercial areas) (as shown in Table 1). Recent research indicates that the traffic patterns and safety are quite different among these roadway

Table I. Descriptive Statistics of the Modeling Variables (N=501)

Variable	Definition	Min	Max	Mean	STD
Crash data					
Total crashes	Total crashes per intersection in 2021–2023	0	161	30.06	25.40
Rear-end crashes	Rear-end crashes per intersection in 2021–2023	0	125	20.40	24.60
Sideswipe crashes	Sideswipe crashes per intersection in 2021–2023	0	63	9.28	10.52
Severe crashes	Fatal and serious injury crashes per intersection in 2021–2023	0	7	0.86	1.32
Vulnerable road user crashes	Pedestrian and bicycle crashes per intersection in 2021–2023	0	14	1.32	1.83
Traffic flow volume					
Log_Major_AADT	The log value of AADT on major road in 2021–2023 (pcu)	6.11	11.18	9.79	0.86
Log_Minor_AADT	The log value of AADT on minor road in 2021–2023 (pcu)	5.30	10.89	8.90	0.00
Log_Major_TruckAADT	The log value of truck AADT on major road in 2021–2023 (pcu)	3.56	9.01	7.18	0.88
Log_Minor_TruckAADT	The log value of truck AADT on minor road in 2021–2023 (pcu)	2.77	8.56	6.36	0.91
Geometric design features					
Legs_4	I:4-legged intersection; 0: 3-legged intersection	0	—	0.73	0.45
Major_lanes	Major road lanes >4 (yes = 1)	0	—	0.20	0.40
Minor_lanes	Minor road lanes >4 (yes = 1)	0	—	0.02	0.14
Major_speed_low	Speed limit on major road <40 mph (yes = 1)	0	—	0.38	0.49
Major_speed_medium	Speed limit on major road 40–50 mph (yes = 1)	0	—	0.59	0.49
Major_speed_high	Speed limit on major road >50 mph (yes = 1)	0	—	0.03	0.8
Minor_speed_low	Speed limit on minor road <40 mph (yes = 1)	0	—	0.66	0.47
Minor_speed_medium	Speed limit on minor road 40–50 mph (yes = 1)	0	—	0.34	0.47
Minor_speed_high	Speed limit on minor road >50 mph (yes = 1)	0	—	0.00	0.06
Major_surface_width	The surface width of major road (feet)	13	96	43.19	17.21
Major_surface_width	The surface width of minor road (feet)	12	69	31.23	10.83
Major_minor_collector	Major road class is minor collector (yes = 1)	0	—	0.02	0.14
Major_major_collector	Major road class is major collector (yes = 1)	0	—	0.24	0.43
Major_minor_arterial	Major road class is minor arterial (yes = 1)	0	—	0.35	0.48
Major_major_arterial	Major road class is major arterial (yes = 1)	0	—	0.39	0.49
Minor_minor_local	Minor road class is local road (yes = 1)	0	—	0.02	0.13
Minor_minor_collector	Minor road class is minor collector (yes = 1)	0	—	0.20	0.40
Minor_major_collector	Minor road class is major collector (yes = 1)	0	—	0.56	0.50
Minor_minor_arterial	Minor road class is minor arterial (yes = 1)	0	—	0.19	0.40
Minor_major_arterial	Minor road class is major arterial (yes = 1)	0	—	0.04	0.19
Major_median_marking	The median type of major road is a traffic marking (yes = 1)	0	—	0.53	0.50
Major_median_separator	The median type of major road is a raised traffic separator (yes = 1)	0	—	0.28	0.45
Major_median_curb	The median type of major road is curb and vegetation (yes = 1)	0	—	0.13	0.34
Minor_median_marking	The median type of minor road is a traffic marking (yes = 1)	0	—	0.71	0.45
Minor_median_separator	The median type of minor road is a raised traffic separator (yes = 1)	0	—	0.8	0.39
Minor_median_curb	The median type of minor road is curb and vegetation (yes = 1)	0	—	0.09	0.29
Socioeconomic variables					
Population	Average population (1,000 people)	0.59	10.66	4.06	1.41
Median_Income	Average median income (\$10,000 per year)	1.28	15.07	5.79	2.52
P_Over65	Percent of population 65 years or older (%)	2.87	78.74	13.57	4.94
P_Under17	Percent of population 17 years or younger (%)	0.42	37.70	19.65	7.17
P_Unemployed	Percent of people aged 16+ years unemployed (%)	0	14.60	3.73	1.95

(continued)

Table 1. (continued)

Variable	Definition	Min	Max	Mean	STD
P_Poverty	Percent of population with income below average poverty level (%)	0.72	74.02	37.56	15.38
P_Uneducation	Percent of people aged 25+ years with less than a high school diploma (%)	0.51	41.90	14.51	7.84
P_Disability	Percent of population with a disability (%)	3.19	62.10	13.30	4.49
P_Mobile_Homes	Percent of total housing units that are mobile homes (%)	0	79.10	4.79	9.94
P_Nocar	Percent of households with no car (%)	0	35.17	10.46	7.46
Commute_Time	Average commute time to work (min)	7.77	39.08	25.09	4.48
Transit_Services	Frequency of transit services per square mile	0	293.02	26.98	36.41
Num_Underserved	Number of underserved communities within the intersection buffer	0	5	1.35	1.17
Road context classifications					
C1 and C2	Intersection at natural or rural area (yes = 1)	0	1	0.05	0.21
C3R	Intersection at suburban residential area (yes = 1)	0	1	0.20	0.40
C3C	Intersection at suburban commercial area (yes = 1)	0	1	0.14	0.35
C4	Intersection at urban general area (yes = 1)	0	1	0.42	0.49
C5	Intersection at urban center area (yes = 1)	0	1	0.08	0.27
C6	Intersection at urban core area (yes = 1)	0	1	0.12	0.33
Visual environment features					
Sky	Proportion of sky visible within the driver's field of vision	0.11	0.47	0.38	0.07
Road	Proportion of road within the driver's field of vision	0.24	0.46	0.42	0.03
Buildings	Proportion of buildings within the driver's field of vision	0	0.33	0.05	0.06
Vegetation	Proportion of vegetation (e.g., trees, grass) within the driver's field of vision	0.02	0.41	0.12	0.06
Vehicle	Proportion of vehicles within the driver's field of vision	0	0.24	0.03	0.02
Walk	Proportion of walk area within the driver's field of vision	0	0.04	0.01	0.01

Note: AADT = annual average daily traffic; STD = standard deviation; pcu = passenger car unit.

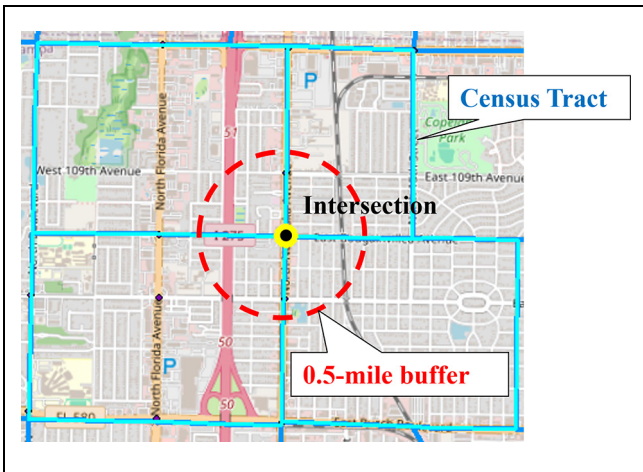


Figure 2. Spatial overlay of census tracts on a 0.5 mi buffer around an intersection.

classifications (32, 33). Therefore, it is essential to combine such features into the intersection crash frequency modeling.

Google Street View (GSV) Images

The GSV panorama platform provides 360-degree surrounding images of Google map locations. To collect the GSV images of each intersection, a Python script was developed to automatically download these images from the HTTP URL form using the Google API (<https://developers.google.com/maps>). For each intersection, the center point was identified as the viewpoint origin, and eight GSV images were obtained to fully capture the drivers' visual perception (as shown in Figure 3). In the GSV system, the heading indicates the compass heading of the camera which ranges from 0° to 360° . There, the eight images are set at headings of 0° (north), 45° (northeast), ..., 315° (northwest) to cover the entire intersection. It is worth noting that other quantities of GSV images (e.g., 2, 4, 16) were also tested, but eight images provided the optimal coverage of the intersection without overlaps. Besides, two other parameters were considered: "fov" is the horizontal field of view for the image, and "pitch" specifies the up or down angle of the camera relative to the data collection vehicle. To get images similar to the drivers' view, the horizontal fov and pitch were

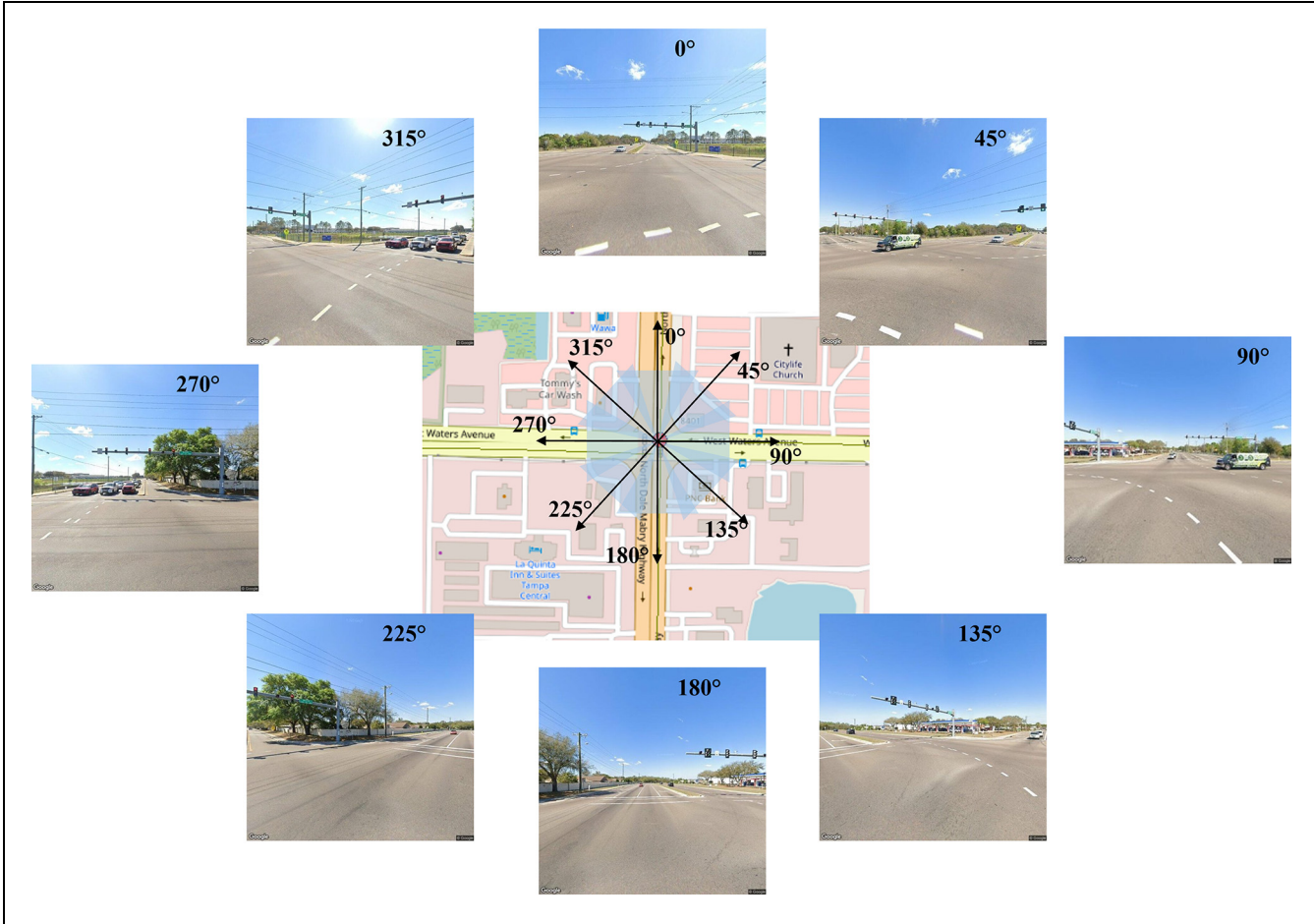


Figure 3. Illustration of Google Street View image collection for each intersection.

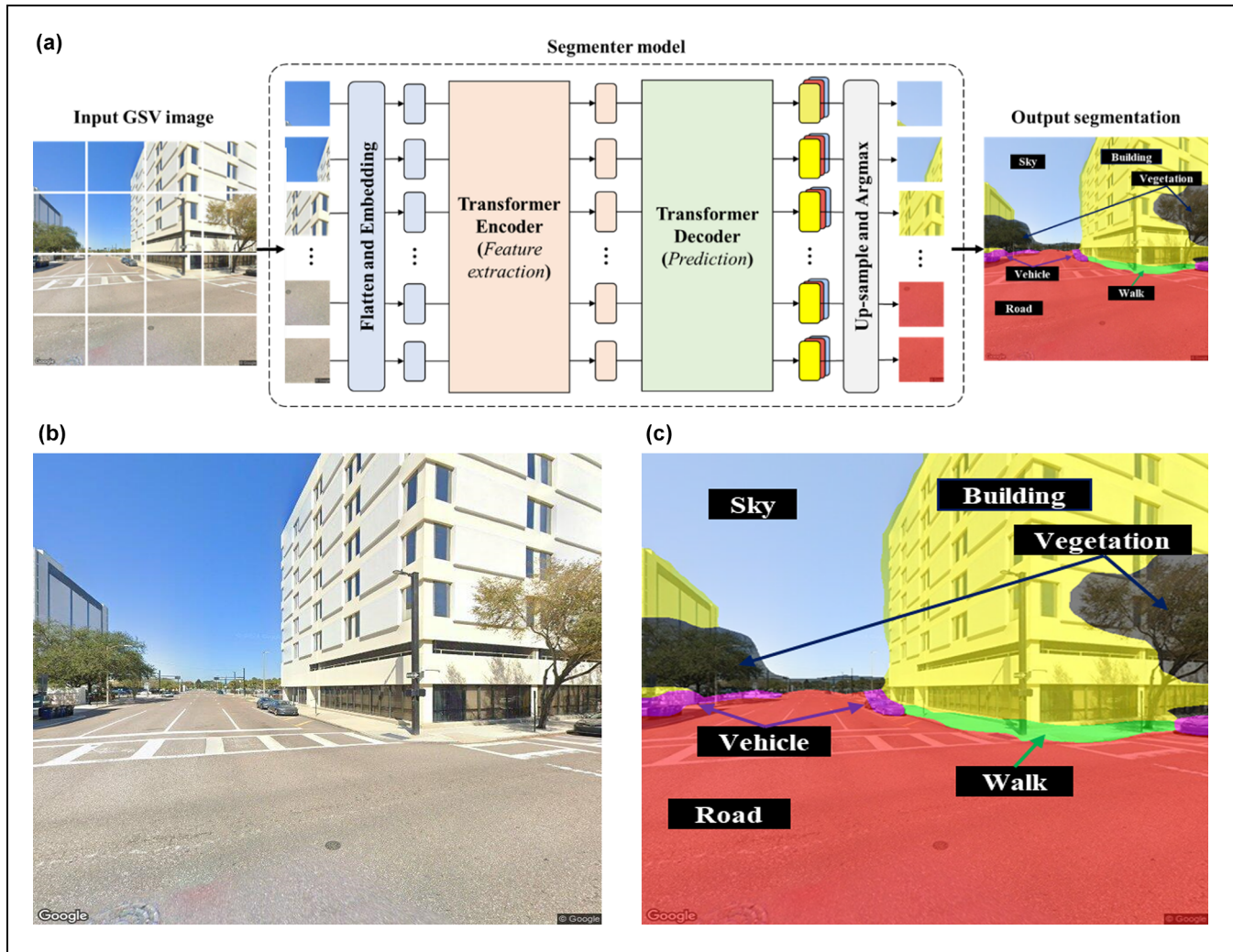


Figure 4. Illustration of semantic segmentation of intersection Google Street View (GSV) images: (a) model structure of Segmenter, (b) raw GSV image (input), and (c) semantic segmentation result (output).

set as 50° and 0° , respectively (25, 34, 35). Finally, a total of $8 \times 501 = 4,008$ GSV images were collected to extract drivers' visual environment features at studied intersections. Note that intersections undergoing construction or renovation were excluded to ensure that the environment features (e.g., buildings and roads) from GSV images at specific time points (e.g., 2023/10/23 as shown on Google maps) remained stable during the study period. Consistent with existing studies, it allows us to reliably use these features to represent typical intersection environment (25, 26, 36).

After obtaining the intersection GSV images, six types of visual environment feature were extracted: the sky, road, surrounding buildings, vegetation, vehicle, and walk area. The progress is detailed in the Methodology section. Overall, Table 1 provides descriptive statistics of crash data and the five categories of explanatory variables.

Methodology

Drivers' Visual Environment Feature Extraction

Recently, semantic segmentation of objects from images has been growing in the field of computer vision, and multiple deep learning methods have been developed (37–39). In this study, “Segmenter,” a transformer-based segmentation model, was used to cluster objects from GSV images. Proposed by Strudel et al., Segmenter can integrate global context information into image segmentation, outperforming convolution-based methods and remaining state-of-the-art (39). Figure 4a illustrates the overall progress of semantic segmentation of an intersection GSV image using the Segmenter model. First, the GSV image is split into a sequence of pixel patches, which are flattened and projected to a series of embeddings. A pre-trained transformer encoder, ViT, takes the

embeddings to extract their contextualized and position features, which are then fed into a transformer decoder to predict their segmentation classes (38). However, we found that directly applying the pre-trained Segmenter resulted in unsatisfactory segmentation accuracy, as it was primarily trained on ImageNet, which includes few transport scenarios. To address this, we introduced a fine-tuning method to enhance domain-specific modeling for traffic safety. Inspired by MaskFormer, we pretrained the model on representations of individual objects, such as buildings and vehicle and traffic signs with exclusive masks, to ensure it learned their critical characteristics (40). Subsequently, we manually labeled 1,000 intersection images in Florida and fine-tuned the model using all segmentation features to improve overall segmentation performance. This approach finally improves the mean segmentation accuracy from 48.7% to 88.9% and mean intersection-over-union from 27.1% to 82.1%, ensuring the accurate semantic segmentation of visual environment features. As shown in Figure 4b and c, a total of six types of object in the drivers' view environment were labeled: sky, road, buildings, vegetation, vehicle, and walk area.

Based on the clustering results, the object type by each pixel can be determined in the image. Since each intersection has eight GSV images, the proportion of object type $Prop_k$ was calculated based on the sum of pixels in the eight images:

$$Prop_k = \frac{P_k}{\sum_{k=1}^6 P_k} = \frac{\sum_{b=1}^8 P_{k,b}}{\sum_{k=1}^6 \sum_{b=1}^8 P_{k,b}} \quad (2)$$

where

$P_{k,b}$ = the number of pixels of object type k in the b -th GSV intersection image,

P_k = the total pixel number of object type k in all intersection images, and

k = sky, road, buildings, vegetation, vehicle, or walk area.

Detailed descriptive statistics of these visual environment features in the modeling data can be seen in Table 1.

Intersection Crash Frequency Modeling

Considering the overdispersion and the preponderance of zeros in crash data, a mixed distribution model, the negative binomial-Lindley (NB-L) model was utilized for intersection crash frequency modeling (3, 27). In addition, the impact of visual environment features may be heterogeneous across intersections because of different traffic situations (23, 36). For example, vegetation may affect drivers' perception in urban area with smaller trees, while it may have a lesser impact at rural intersections characterized by dense tree cover. Therefore, the RPNB-

L model was further developed to capture the unobserved heterogeneities and thus improve model fitness (41, 42).

NB-L Model. The NB-L model has been widely used for crash frequency modeling because of its superior fitting ability of over-dispersed crash data. It can be seen as a mixture of negative binomial (NB) and Lindley distributions. Let Y_i be the crash counts for intersection i ($1, 2, \dots, N = 501$); the NB-L model can be formulated in the context of generalized linear models as:

$$P(Y_i = y_i | \mu_i, \phi, \theta) = \int NB(y_i | \phi, \varepsilon_i \mu_i) Lindley(\varepsilon_i | \theta) d\varepsilon_i \quad (3)$$

In the above formula, the mean of the NB distribution, μ_i , is multiplied by a random error term ε_i . The dispersion parameter of this distribution is denoted by ϕ . The random error term ε_i follows a Lindley distribution with parameter θ . Given the crash frequency Y_i follows such NB-L distribution, its mean function can be expressed as:

$$E(Y_i = y_i) = \mu_i \times E(\varepsilon_i) \quad (4)$$

Here, $\mu_i = \exp(\beta_0 + \sum_{j=1}^q \beta_j x_{ij})$
where

β_0 = the intercept,

x_{ij} = the j -th covariate at i intersection, and

β_j = the regression coefficient to be estimated.

According to Zamani and Ismail, 2010, the mean of Lindley distribution is defined as (43):

$$E(\varepsilon_i) = \frac{2 + \theta}{\theta(1 + \theta)} \quad (5)$$

Thus, Equation 4 can be expressed as:

$$\begin{aligned} E(Y_i = y_i) &= \exp\left(\beta_0 + \sum_{j=1}^q \beta_j x_{ij}\right) \times \frac{2 + \theta}{\theta(1 + \theta)} \\ &= \exp\left(\beta_0 + \sum_{j=1}^q \beta_j x_{ij} + \ln\left(\frac{2 + \theta}{\theta(1 + \theta)}\right)\right) \end{aligned} \quad (6)$$

As the Lindley distribution is a mixture of two gamma distributions, its hierarchical representation can be reformulated as follows:

$$\varepsilon_i | \theta \sim \sum Gamma(1 + z_i, \theta) Bernoulli(z_i | \frac{1}{1 + \theta}) \quad (7)$$

Considering the Bayesian framework, the multi-level hierarchical structure for the NB-L model can be parameterized as follows:

$$\left. \begin{array}{l} Y_i \sim NB(y_i | \varepsilon_i \mu_i, \phi) \\ \mu_i = \exp(\beta_0 + \sum_{j=1}^q \beta_j x_{ij}) \\ \varepsilon_i | \theta \sim Gamma(1 + z_i, \theta) \\ z_i \sim Bernoulli(z_i | \frac{1}{1+\theta}) \end{array} \right\} \quad (8)$$

Following existing studies, the shape parameter θ in the gamma distribution follows a Bernoulli distribution with a probability parameter of $1/(1 + \theta) \sim beta(N/3, N/2)$ (44). The dispersion parameter ϕ is assumed to be follow a uniform distribution and the regression coefficient β_j follows a normal distribution.

RPNB-L Model. To account for unobserved heterogeneity, a mixed parameter model, RPNB-L, was developed. In the context of the RPNB-L model, the regression coefficient β_{ij} is assumed to be random. It can be seen as a combination of fixed terms β_j and random terms w_{ij} :

$$\beta_{ij} = \beta_j + w_{ij} \quad (9)$$

Here, the random term w_{ij} is assumed to follow a predefined distribution, such as a normal distribution with zero mean and a standard deviation of σ_j for j -th covariate x_{ij} .

However, β_{ij} is regarded as a random parameter only if its estimated variance improves the model's goodness of fit. Otherwise, the parameter is considered to be a fixed parameter β_j . Therefore, the RPNB-L can be parameterized in the Bayesian framework:

$$\left. \begin{array}{l} Y_i \sim NB(y_i | \varepsilon_i \mu_i, \phi) \\ \mu_i = \exp(\beta_0' + \sum_{j=1}^q \beta_{ij} x_{i,j}) \\ \varepsilon_i | \theta \sim Gamma(1 + z_i, \theta) \\ z_i \sim Bernoulli(z_i | \frac{1}{1+\theta}) \\ \beta_{ij} = \beta_j + w_{ij} \\ w_{ij} \sim Normal(0, \sigma_j^2) \end{array} \right\} \quad (10)$$

In earlier studies, different distributions, such as normal, lognormal, uniform, gamma, and so forth, were applied, and the normal distribution was found to provide the best statistical fit for random parameters (41, 42, 45). Therefore, normal distribution was applied in this study:

$$\beta_{ij} \sim Normal(\beta_j, \sigma_j^2), 1/\sigma_j^2 \sim Gamma(0.001, 0.001) \quad (11)$$

Model Goodness of Fit Measures. Referring to existing studies, four measures were utilized to comprehensively compare the model goodness of fit in this study, as discussed in the following sub-sections (41, 42, 45).

Deviance Information Criterion (DIC). DIC was considered as a local goodness of fit measure to compare the

estimated models. DIC is the hierarchical modeling generalization of the Akaike information criterion and Bayesian information criterion which penalize the larger parameter model. Mathematically, DIC can be formulated as follows:

$$DIC = \overline{D(\delta)} + P_D \quad (12)$$

where

$$\overline{D(\delta)} = -2\log L,$$

L = the likelihood of model convergence for parameter estimates, and

$P_D = \overline{D(\delta)} - D(\hat{\delta})$ = the effective number of parameters reflecting the complexity of the model (deviance $D(\delta)$ is evaluated at the posterior summary of the total number of parameters δ).

Generally, the model with lower DIC is considered superior among the candidate models.

McFadden's pseudo R^2 . McFadden's pseudo R^2 was also used to compare the model goodness of fit, which can be estimated as follows (46):

$$R^2 = 1 - \frac{L(\delta)}{L(C)} \quad (13)$$

where

$L(\delta)$ = the log-likelihood value of the full model, and

$L(C)$ = the log-likelihood value of the constant-only model.

In contrast to DIC, the higher the value of McFadden's pseudo R^2 , the better the model goodness of fit is.

Mean Absolute Error (MAE) and Mean Squared Error (MSE). To evaluate the prediction performance of candidate models, two global goodness of fit measures are the mean absolute error (MAE) and mean squared error (MSE). For MAE and MSE, the lower the values of these measures, the better the model's prediction performance. These two measures can be calculated as follow:

$$MAE = \frac{1}{N} \sum |Y_i - y_i| \quad (14)$$

$$MSE = \frac{1}{N} \sum (Y_i - y_i)^2 \quad (15)$$

where

N = the number of observations,

Y_i = the observed crash count for intersection i , and

y_i = the predicted crash count for intersection i .

Table 2. Comparison of Estimation Results of Negative Binomial (NB), Negative Binomial-Lindley (NB-L), and Random Parameter Negative Binomial-Lindley (RPNB-L) Models (N = 501)

Explanatory variables	NB			NB-L			RPNB-L		
	Coef.	Std dev.	Sig. code	Coef.	Std dev.	Sig. code	Coef.	Std dev.	Sig. code
Intercept	-1.013	0.566	*	-6.810	0.903	***	-4.144	1.569	***
Traffic flow volume									
Log_Major_AADT	0.254	0.042	***	0.263	0.058	***	0.216	0.064	***
Log_Minor_AADT	0.180	0.032	***	0.194	0.042	***	0.171	0.058	***
Geometric design features									
Legs_4	0.318	0.064	***	0.325	0.087	***	0.299	0.114	***
Minor_lanes	0.444	0.177	*	0.458	0.254	*	0.525	0.272	*
Major_minor_arterial	0.265	0.075	***	0.271	0.106	**	0.362	0.100	***
Major_major_arterial	0.409	0.090	***	0.403	0.126	***	0.596	0.117	***
Socioeconomic variables									
Number_Underserved	0.097	0.023	***	0.101	0.034	***	0.097	0.039	**
P_mobile_Homes	-0.009	0.003	**	-0.009	0.004	**	-0.008	0.004	**
Visual environment features									
Building	-2.675	0.478	***	-2.770	0.652	***	-2.304	0.951	**
STD.DEV of building	na	na	na	na	na	na	0.941	0.534	*
Vegetation	-2.896	0.549	***	-2.838	0.713	***	-2.403	1.007	**
STD.DEV of Vegetation	na	na	na	na	na	na	0.398	0.218	*
Model parameters									
Dispersion parameter (ϕ)	3.745	0.284	***	14.670	2.780	***	14.550	2.808	***
Lindley parameter (θ)	na	na	na	1.176	0.112	***	1.169	0.117	***
Model goodness of fit measures									
DIC		3,983.070			3,742.720			3,656.980	
McFadden's pseudo R ²		0.579			0.789			0.792	
MAE		11.840			7.449			7.411	
MSE		271.300			137.400			134.300	

Note: AADT = annual average daily traffic; DIC = deviance information criterion; MAE = mean absolute error; MSE = mean squared error; na = not applicable.

*90% confidence level.

**95% confidence level.

***99% confidence level.

Results

Model Performance Comparison

In this study, the proposed NB-L and RPNB-L models were estimated under the Bayesian framework in WinBUGS software (47). For comparison purposes, the traditional NB model was also developed in the same framework. Referring to existing studies, a total of three Markov chains were considered while estimating these models (41, 48, 49). For each Markov chain, 80,000 iterations were performed; the first 20,000 samples were the burn-in samples. To minimize the variable correlations, Pearson's correlation test was conducted, and the highly correlated variables were excluded to avoid multicollinearity. To ensure the convergence of models, the Gelman-Rubin statistics threshold value was selected as less than 1.1 and the Monte Carlo error for estimated parameter was adopted as less than 3% of the posterior standard deviation (41, 50). Here, the response variable is the total crash frequency among the 3 years.

After the correlated variable filtering and model fitting, a total of 10 variables were found to significantly influence the intersection crashes. Additionally, the variance inflation factor for each variable was computed, and none exceeded the threshold of 5, indicating low multicollinearity in the models. Table 2 summarizes the estimation of their parameters for the three mentioned models: NB, NB-L, and RPNB-L. From the goodness of fit perspective, the results shows that the RPNB-L model provides the lowest DIC value (3,656.980) among the three models, demonstrating it to be the superior statistically fitted model. Meanwhile, the RPNB-L model also provides the highest McFadden's pseudo R². Compared with the NB and NB-L models, the improvement of McFadden's pseudo R² are $(0.792 - 0.579)/0.579 = 36.93\%$ and $(0.792 - 0.789)/0.789 = 0.39\%$, respectively. It is worth mentioning that the estimated DIC and R² can be influenced by model parameterization. Therefore, the same model parameterization was adopted to ensure an adequate comparison among the estimated models. As for the MAE and MSE, the RPNB-L model still shows the best

Table 3. Estimation Results of Models with and without Visual Features (N = 501)

Explanatory variable	Model with visual features			Model without visual features		
	Coef.	Std dev.	Sig. code	Coef.	Std error	Sig. code
Intercept	-4.144	1.569	***	-4.945	1.527	***
Traffic flow volume						
Log_Major_AADT	0.216	0.064	***	0.207	0.061	***
Log_Minor_AADT	0.171	0.058	***	0.153	0.039	***
Geometric design features						
Legs_4	0.299	0.114	***	0.364	0.096	***
Major_lanes	na	na	na	0.326	0.119	***
Minor_lanes	0.525	0.272	***	na	na	na
Major_minor_arterial	0.362	0.100	*	0.321	0.100	***
Major_major_arterial	0.596	0.117	***	0.479	0.122	***
Minor_major_collector	na	na	na	0.292	0.081	***
STD.DEV of Minor_major_collector	na	na	na	0.058	0.028	*
Minor_minor_arterial	na	na	na	0.292	0.081	***
Socioeconomic variables						
Num_Underserved	0.097	0.039	**	0.110	0.031	***
P_Mobile_Homes	-0.008	0.004	**	na	na	na
Road context classifications						
C1 and C2	na	na	na	-0.342	0.189	**
Visual environment features						
Buildings	-2.304	0.951	**	na	na	na
STD.DEV of Building	0.941	0.534	*	na	na	na
Vegetation	-2.403	1.007	**	na	na	na
STD.DEV of Vegetation	0.398	0.218	*	na	na	na
Model parameters						
Dispersion parameter (ϕ)	14.550	2.808	***	14.240	2.636	***
Lindley parameter (θ)	1.169	0.117	***	1.177	0.118	***
Model goodness of fit measures						
DIC		3,656.980			3,800.910	
McFadden's pseudo R ²		0.792			0.786	
MAE		7.411			7.509	
MSE		134.300			137.400	

Note: DIC = deviance information criterion; MAE = mean absolute error; MSE = mean squared error; na = not applicable.

*90% confidence level.

**95% confidence level.

***99% confidence level.

performance among the three models with the lowest MAE (7.411) and MSE (134.300). Compared with the regular NB model, the MAE and MSE values were significantly reduced by $|7.411-11.840| / 11.840 = 37.41\%$ and $|134.300-271.300| / 271.300 = 50.50\%$, respectively. Furthermore, the estimated Lindley parameters (θ) are significant at the 95% confidence level in the RPNB-L model, indicating that the introduction of parameter randomness could help improve model fit better under the Lindley distributions. Therefore, it could be concluded that the RPNB-L model outperforms the traditional NB and fixed coefficient NB-L models by incorporating the mixed distribution, as well as enabling the posterior parameter estimates of explanatory variables to vary from one observation to another.

To further assess the benefit of visual environment features, two RPNB-L models—one including the visual

environment features and one excluding them—were compared. Their estimated results are shown in Table 3. Without visual environment features, a total of 10 variables (e.g., Log_Major_AADT, Log_Minor_AADT, Legs_4) are found to be significantly correlated with the intersection crash frequency. However, only six explanatory variables (e.g., Log_Major_AADT and Log_Minor_AADT) remain significant with the inclusion of visual environment features. Compared with the model without visual features, the inclusion of visual environment features reduced the DIC by $3800.910 - 3656.980 = 143.93 > 10$, indicating a significant improvement in model fit at the 95% confidence level. As a result, the model demonstrated a higher McFadden's pseudo R², lower MAE, and lower MSE. These results confirm that introducing visual environment features effectively captures the important impacts

of drivers' visual perception of the surrounding environment, therefore enhancing both model fit and prediction performance.

Total Intersection Crash Frequency Contributing Factors

Given that the RPNB-L model archives the best model goodness of fit, the significant contributing factors can be identified through its estimation results. Based on the estimated parameters of RPNB-L in Table 2, conclusions can be drawn, as presented in the following subsections.

Traffic Flow Characteristics. Both the natural logarithm of AADT on major and minor roads (*Log_Major/Minor_AADT*) are significantly positive with intersection crash frequency at the 99% confidence level. It means that higher traffic volume, whether on major or minor roads, leads to greater exposure to risky vehicle interactions, thereby being directly related to the occurrence of more intersection crashes (19, 27).

Geometric Design Features. Four geometric design variables (i.e., *Legs_4*, *Minor_lanes*, *Major_minor_arterial*, and *Major_major_arterial*) show positive correlation with intersection crash frequency. These results indicate that intersections with four legs and more than four lanes on minor roads experience more crashes because of the increased number of potential traffic conflict points, aligning well with previous studies (17, 18). Additionally, intersections on major roads that are classified as minor or major arterials also have a higher likelihood of crashes. It may be because arterial roads typically have higher speed limits, providing less reaction time for drivers and more complex traffic compositions (e.g., trucks and motorcycles), as suggested in and Gu et al. (51).

Socioeconomic Variables. The number of underserved communities surrounding intersections (*Num_Underserved*) is significantly positively correlated with intersection crash frequency. According to the U.S. DOT ETC Project, underserved communities suffer from high social vulnerability (e.g., high poverty, low educational attainment, insufficient local jobs, high inequality, and low homeownership). The results indicate that such underserved communities suffer more intersection crashes and more serious safety issues than other areas, highlighting the need for more attention, as suggested by recent studies (20, 31). Interestingly, the percent of mobile homes (*P_Mobile_Homes*) shows a negative correlation with total intersection crashes; this is the same as the findings of Patwary et al. (31). It indicates that the places with a higher proportion of mobile houses often have

fewer residents and daily activities, thereby decreasing driving interaction and human-vehicle conflicts at intersections.

Visual Environment Features. Two visual environment variables (i.e., buildings and vegetation) present significantly negative correlation with total crash frequency at 95% confidence level. The coefficients for the proportion of buildings and vegetation within a driver's field of view have means of -2.304 and -2.403 , respectively, showing that an increase in the proportion of vegetation and buildings in the drivers' point of view positively correlates with the number of crashes, consistent with existing studies (21, 25). Moreover, the estimated coefficients of them were found to be randomly distributed with standard deviations of 0.941 and 0.398 at 90% confidence level, respectively. This indicates that their impacts may vary among different intersections and the variability associated with buildings is more pronounced than that of vegetation.

- For vegetation, more surrounding vegetation, especially roadside trees, can make drivers feel a narrow road and exercise more caution when approaching intersections (52). Meanwhile, roadside vegetation is found to have a positive psychological effect to reduce the stress and anxiety of drivers, thereby reducing speeding behaviors and crashes (21).
- As for buildings, existing studies show that the presence of buildings can indicate more pedestrian activity and thus requires more caution by drivers. More buildings may make drivers slow down and pay more attention to crowded pedestrians and vehicles, therefore leading to reduced crashes (21, 53, 54).

Figure 5 further illustrates the relationships between intersection crash frequency and various visual environment features. Figure 5a clearly demonstrate that intersections with higher crash frequencies (red dots) generally exhibit lesser vegetation and surrounding buildings. In contrast, they tend to have larger visible road surfaces and a higher proportion of open sky (as shown in Figure 5b to d). According to existing studies, extensive road areas typically correspond to wider roadways, while greater sky visibility suggests more open roadway spaces (21, 25, 26). Such visual environments may encourage higher driving speeds and reduced caution when approaching intersections. Conversely, more vegetation and buildings may serve as visual cues for drivers to perceive a more urban or populated area, prompting them to drive at lower speeds with more focus.

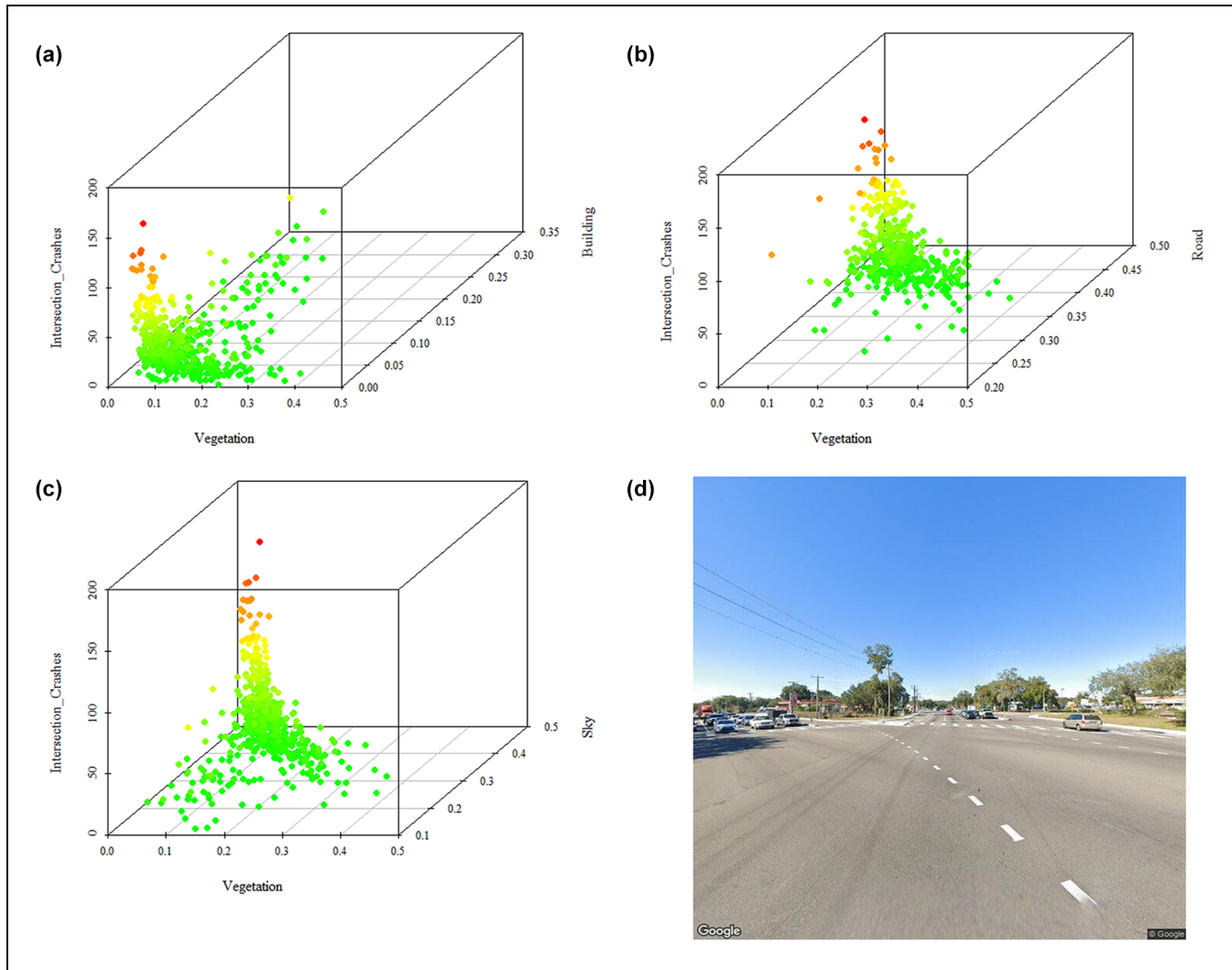


Figure 5. Scatter plots of intersection crashes versus visual environment features: (a) vegetation and buildings, (b) vegetation and roads, (c) vegetation and sky, and (d) high-crash-frequency intersection.

Note: red dots = intersections with higher crash frequencies.

Specific Intersection Crash Frequency Contributing Factors

Existing studies have shown that different types of intersection crash may suffer different problems and contributing factors (12, 15, 55). To identify the contributing factors for specific types of intersection crash, four RPBN-L models were further developed with the target variables of the frequency of rear-end, sideswipe, severe, and vulnerable road user crashes. Rear-end and sideswipe are two common types of crash, accounting for about 60%–70% of intersection crashes. Severe crash modeling aims to analyze critical issues related to fatal and serious crashes, which are the main focus of the Vision Zero Plan (56). Vulnerable road user crashes include pedestrian- and bicycle-involved crashes, and the

corresponding modeling can help identify countermeasures to protect the safety of vulnerable road users. Table 4 presents the estimated results for the four specific intersection crash frequency models, clearly demonstrating the different contributing factors to each type of intersection crash.

Traffic Flow Characteristics. The traffic volume on major roads (Log_Major_AADT) remains significantly positively correlated to all four types of crash. It indicates that traffic volume at major roads serves as the main exposure to vehicles' interaction, thereby leading to more crashes. The traffic volume on minor roads (Log_Minor_AADT) is significantly positively correlated to only rear-end and severe crashes, which is reasonable

Table 4. Estimation Results for Four Specific Types of Crash Frequency Model ($N=501$)

Variable type	Rear-end crashes	Sideswipe crashes	Severe crashes	Vulnerable road user crashes
Intercept	-8.856***	-6.995***	-5.160***	-5.259***
Traffic flow volume	Log_Major_AADT: 0.527*** Log_Minor_AADT: 0.159*** Legs_4: 0.277*** Minor_speed_medium: 0.239***	Log_Major_AADT: 0.225*** Log_Minor_AADT: 0.241*** Legs_4: 0.563*** Major_lanes: 0.292***	Log_Major_AADT: 0.529*** Minor_speed_high: 0.664***	Log_Major_AADT: 0.394*** Major_major_collector: -0.567***
Geometric design features	Major_major_arterial: 0.385*** Minor_median_Separator: 0.350***	Major_minor_arterial: 0.520*** Major_major_arterial: 0.652*** Minor_minor_arterial: 0.331**		
Socioeconomic variables	Num_Underserved: 0.059* Population: 0.060***	Num_Underserved: 0.233***	Num_Underserved: 0.186***	Num_Underserved: 0.186***
Road context classifications		C1 and C2: -0.643** C4: 0.226** C5: 0.416*** (0.241*) C6: 0.667*** (0.666**) Vegetation: -4.792***	C1&C2: -2.351**	
Visual environment features	Road: 0.721*** (0.127*) Vehicle: 5.260*** (1.055*) Building: -2.875*** (1.300**)	Road: 0.465*** (1.465*) Building: -2.971*** (1.650*)	Road: 3.135*** (0.302*) Vehicle: 4.599*** (1.392**)	
Model parameters				
Dispersion parameter (ϕ)	12.530*** 1.302***	10.250*** 1.334***	7.273*** 1.483***	8.001*** 1.462***
Lindley parameter (H)				
Model goodness of fit measures				
DIC	3299,000	1975,310	1107,300	1386,260
McFadden's Pseudo R ²	0.833	0.751	0.433	0.534
MAE	5.594	3.157	0.642	0.828
MSE	100,900	27,500	0.993	1.555

Note: AADT = annual average daily traffic; DIC = deviance information criterion; MAE = mean absolute error; MSE = mean squared error.

* 90% confidence level.

** 95% confidence level.

*** 99% confidence level.

Values in parentheses are the estimated standard deviations of the random parameters.

as traffic from minor roads also increase the vehicle volume at intersections, thereby contributing to the exposure of these two types.

Geometric Design Features. The significant geometric design features substantially differ among these four models. Overall, 4-leg intersection (Legs_4) and major-arterial approach (Major_major_arterial) show positive correlation with rear-end and sideswipe crashes. More approach legs and a higher major road class reflect more traffic and larger road widths, which consequently bring more potential vehicle-to-vehicle conflicts of rear-end and sideswipe crashes. Specific features contribute to different types of crashes.

- For rear-end crashes, the medium speed limit on minor roads (Minor_speed_medium) and the presence of raised separators in the median of minor roads (Minor_median_Separator) are two significant factors that positively correlate with the frequency of rear-end crashes. Compared with a low speed limit (<40 mph), a speed limit of 40–50 mph is quite high for a minor road. At such high speeds, drivers have less reaction time and a narrow field of view, making it more difficult to brake in time to avoid rear-end crashes with leading cars (21, 25, 57). Additionally, the raised traffic separators on minor roads become less conspicuous than the wide medians with curbs and vegetation. Therefore, drivers may overlook and run over them, resulting in sudden braking and rear-end crashes. Roads with raised traffic separators often have higher road grade with more lanes and traffic than those with only traffic markings, thus leading to an increased frequency of rear-end crashes.
- For sideswipe crashes, intersections with multiple lanes (>4) on major roads (Major_lanes) and minor arterial approaches (Major_minor_arterial & Minor_minor_arterial) have more sideswipe crashes. This indicates that more lanes and minor arterials have more traffic and changing lanes, thus causing more sideswipe crashes.
- For vulnerable road user crashes, interestingly, intersections where the major road is a major collector (Major_major_collector) are estimated to have fewer pedestrian and bicycle crashes. This may be because major collectors are equipped with multiple vulnerable road user protection infrastructure (e.g., pedestrian crosswalks) and do not have as many pedestrians or bicycles as arterials.

Speed Limit. Intersections with a high speed limit on minor roads (Minor_speed_high) are found to have significantly more severe crashes. As concluded by

numerous prior studies, a high speed limit (>50 mph) makes the traffic speed at a high level, which bring serious impact forces during crashes to both drivers and non-motor users, significantly increasing the risk of serious injury and fatality (21, 58).

Socioeconomic Variables. The number of underserved communities surrounding intersections (Num_Underserved) shows a significantly positive correlation with all types of crash, except for sideswipe crashes. According to the Hillsborough ETC dataset, the unemployed and undereducated percentages in underserved communities are 4.21% and 18.29%, respectively, approximately 1.48 and 2.65 times higher than those in normal areas (2.84% and 6.91%), respectively. Existing studies show that a large unemployed and undereducated population tends to have higher levels of pedestrian activity, which leads to more conflicts between vehicles and pedestrians (31, 59). The medium income in underserved communities is \$45,023 per year, significantly lower than that in normal areas (\$78,259). Also the percentage of uninsured population in underserved communities is 22.19%, much higher than in normal areas (13.86%). Thus, injured people in such areas may not receive immediate and proper treatment because of poverty and lack of adequate medical insurance, therefore contributing to the increase in the number of crashes which have severe consequences (31). These results further demonstrate poor traffic safety in underserved communities, and the need for increased attention and government support. Population size is found to be significantly associated with high rear-end crash frequency, as more people may generate more crossing pedestrians and vehicles, which can lead to sudden braking of vehicles and rear-end crashes (60).

Road Context Classifications. The context class of the corridors is a critical feature for sideswipe and vulnerable road user crashes. Taking the suburban (C3C/R) as a baseline, intersections in rural areas (C1 and C2) are estimated to have fewer sideswipe crashes. In contrast, intersections in urban areas (C4/C5/C6) show a higher frequency of sideswipe crashes. This reveals that sideswipe crashes are more likely to occur at urban areas as there are more turning traffic and changing lanes at intersections. Intersections in rural areas are estimated to have fewer vulnerable road user crashes as there are fewer pedestrians or bicycle users.

Visual Environment Features. Results show that different visual environment features are significant in all four models, further emphasizing their importance in intersection crash analysis. Except for the sideswipe crash model, the estimated coefficients of these features still follow



Figure 6. Illustration of intersections with different visual environment features: (a) high proportion of vegetation, (b) high proportion of buildings, (c) high proportion of road, and (d) high proportion of vehicles.

random distributions, meaning that their impacts are not fixed but vary across different intersections. Some of the significant findings are shown below:

- The proportions of vegetation and buildings at the intersection environment are negatively correlated with the frequency of rear-end, sideswipe, and severe crashes, revealing their positive effects on traffic safety (21, 25, 33). As expected, more vegetation and buildings at intersections can cause drivers to slow down and stay attentive to surrounding traffic participants, thus greatly reducing the frequency of severe crashes (25, 53, 54). This

suggests that, to improve intersection safety, it is beneficial to strategically add visual elements such as vegetation (e.g., trees and landscaping) or architectural features alongside the road (as shown in Figure 6a and b). These elements can alter drivers' perception of road width, creating an impression of narrower lanes and thus promoting slower, safer driving.

- The proportion of road and vehicles are positively correlated to the frequency of rear-end and vulnerable road user crashes. The proportion of road visible to drivers serves as an indicator of the amount of open road space. As suggested in

previous studies, open road space may encourage drivers to speed, and reduce their visibility of surrounding traffic participants (Figure 6c) (21, 51). Therefore, large road spaces may decrease drivers' attention and lead them to ignore vehicles, pedestrians, and bicyclists, causing more rear-end and vulnerable road user crashes. As far as vehicles are concerned, on the one hand, a high proportion of vehicles directly reflects a high traffic volume at intersections. On the other hand, more vehicles in the drivers' view also cause a more complex visual environment, increasing driver pressure and leading to more traffic conflicts and rear-end crashes. Furthermore (as shown in Figure 6d), a high proportion of vehicles may represent many parked vehicles along the roadway, which can seriously block the visibility of pedestrians or bicycles to drivers, therefore leading to a higher frequency of vulnerable road user crashes.

Conclusions

Existing intersection crash frequency studies primarily consider macro and static infrastructure and traffic conditions (24, 28, 55). However, drivers' micro-visual perception of surrounding environments at intersections also strongly affects their driving behavior and safety, and this has not been adequately investigated yet. To address such gap, this study developed a novel computer vision model to extract drivers' visual environment features at intersections from open-source GSV images. For each intersection, eight-angle GSV images were collected to capture the entire intersection environment. A total of six types of object in the images were segmented: sky, road, buildings, vegetation, vehicles, and walk area. The pixel proportion of these objects was aggregated to measure these features in the drivers' visual environment. To analyze their heterogeneous influence on intersection safety, these visual environment features, along with various geometric designs, roadway traffic, and socioeconomic features, were combined into a RPNB-L model for crash frequency modeling.

Data from 501 signalized intersections in Hillsborough County were used for this empirical study. From the model results, the main conclusions can be summarized as:

- 1) By utilizing the mixed distribution to capture the heterogeneous effects of visual environment features, the RPNB-L model outperformed the traditional NB and fixed coefficient NB-L models.
- 2) Compared with the model without visual environment features, the inclusion of these features

represents the important impacts of drivers' visual perception of the intersection environment, therefore resulting in better model fitness, as reflected by lower DIC, MAE, and MSE values, and a higher McFadden's pseudo R^2 .

- 3) For total crashes, intersections near more underserved communities would suffer more crashes. Two visual environment features (i.e., buildings and vegetation) are significantly negatively correlated with crash frequency, as more vegetation and buildings may prompt drivers to drive at lower speeds and more carefully.
- 4) Different types of intersection crash have different contributing factors. Overall, a high proportion of buildings and vegetation at intersections helps to reduce the rear-end, sideswipe, and severe crashes. However, the proportions of road and vehicles are highly positively correlated with the frequency of rear-end and vulnerable road user crashes, likely because they increase visual complexity and may obstruct drivers' vision.

The findings from this study could help transportation agencies implement effective policies for preventing crash occurrences and improving intersection safety. For example, it is beneficial to strategically add vegetation (e.g., trees and landscaping) and architectural features alongside the intersection approaches, as this can promote traffic calming and reduce drivers' speed (61, 62). Also, specific warning signs can be placed at open and crowded intersections to remind drivers to avoid distractions and drive carefully, therefore enhancing safety at intersections. However, though this study extensively analyzed the impacts of drivers' visual environment features on intersection safety, there is some scope for future work. First, more detailed features (e.g., transit stations, roadside parking), which may potentially affect drivers' visual perception and interaction, can be identified to further investigate their impacts on intersection safety and provide more interesting insights. Second, more advanced statistical and machine learning methods can be employed to discover the non-linear and heterogeneous relationships between these contributing factors and intersection crashes (63, 64). Third, this study developed univariate models to analyze impact factors at different crash types separately. Recently, advanced models (e.g., multivariate model, model with heterogeneity in means and variances, temporal-spatial model) offer promising opportunities for future research to explore complex heterogeneity among crash data (42, 65–67).

Acknowledgments

The authors thank Dr. Chenzhu Wang for his great suggestions on this study.

Author Contributions

The authors confirm their contribution to the paper as follows: study conception and design: L. Han, Y. Joo, M. Abdel-Aty; data collection: L. Han, Y. Joo, S. Zhai, D. Wang; analysis and interpretation of results: L. Han, M. Abdel-Aty; draft manuscript preparation: L. Han, Y. Joo, M. Abdel-Aty, S. Zhai, D. Wang. All authors reviewed the results and approved the final version of the manuscript.

Declaration of Conflicting Interests

The author(s) declared no potential conflicts of interest with respect to the research, authorship, and/or publication of this article.

Funding

The author(s) disclosed receipt of the following financial support for the research, authorship, and/or publication of this article: This study is part of the initial analysis of an SS4A grant to Hillsborough Metropolitan Planning Organization. This work is also partially supported by the Center for Smart Streetscapes, an NSF Engineering Research Center, under grant agreement EEC-2133516.

ORCID IDs

Lei Han  <https://orcid.org/0000-0002-2976-0762>
 Mohamed Abdel-Aty  <https://orcid.org/0000-0002-4838-1573>
 Yang-Jun Joo  <https://orcid.org/0000-0003-2319-0874>
 Dongdong Wang  <https://orcid.org/0000-0001-7278-5415>

Data Accessibility Statement

The authors do not have permission to share data.

References

- Intersection Safety. FHWA. <https://highways.dot.gov/safety/intersection-safety/about>. Accessed July 17, 2024.
- About Intersection Safety. FHWA. <https://highways.dot.gov/safety/intersection-safety/about>. Accessed July 17, 2024.
- Manirul Islam, S., S. Washington, J. Kim, and M. Haque. A Comprehensive Analysis on the Effects of Signal Strategies, Intersection Geometry, and Traffic Operation Factors on Right-Turn Crashes at Signalised Intersections: An Application of Hierarchical Crash Frequency Model. *Accident Analysis & Prevention*, Vol. 171, 2022, p. 106663. <https://doi.org/10.1016/j.aap.2022.106663>.
- Gu, Y., D. Liu, R. Arvin, A. J. Khattak, and L. D. Han. Predicting Intersection Crash Frequency Using Connected Vehicle Data: A Framework for Geographical Random Forest. *Accident Analysis & Prevention*, Vol. 179, 2023, p. 106880. <https://doi.org/10.1016/j.aap.2022.106880>.
- Kabir, R., S. M. Remias, S. M. Lavrenz, and J. Waddell. Assessing the Impact of Traffic Signal Performance on Crash Frequency for Signalized Intersections Along Urban Arterials: A Random Parameter Modeling Approach. *Accident Analysis & Prevention*, Vol. 149, 2021, p. 105868. <https://doi.org/10.1016/j.aap.2020.105868>.
- Yuan, J., and M. Abdel-Aty. Approach-Level Real-Time Crash Risk Analysis for Signalized Intersections. *Accident Analysis & Prevention*, Vol. 119, 2018, pp. 274–289. <https://doi.org/10.1016/j.aap.2018.07.031>.
- Wu, P., T. Chen, Y. Diew Wong, X. Meng, X. Wang, and W. Liu. Exploring Key Spatio-Temporal Features of Crash Risk Hot Spots on Urban Road Network: A Machine Learning Approach. *Transportation Research Part A: Policy and Practice*, Vol. 173, 2023, p. 103717. <https://doi.org/10.1016/j.tra.2023.103717>.
- Zheng, Q., F. Sharmeen, C. Xu, and P. Liu. Assessing Regional Road Traffic Safety in Sweden Through Dynamic Panel Data Analysis: Influence of the Planned Innovative Policies and the Unplanned COVID-19 Pandemic. *Transportation Research Part A: Policy and Practice*, Vol. 179, 2024, p. 103918. <https://doi.org/10.1016/j.tra.2023.103918>.
- Guo, F., X. Wang, and M. A. Abdel-Aty. Modeling Signalized Intersection Safety with Corridor-Level Spatial Correlations. *Accident Analysis & Prevention*, Vol. 42, No. 1, 2010, pp. 84–92. <https://doi.org/10.1016/j.aap.2009.07.005>.
- Dong, C., D. B. Clarke, X. Yan, A. Khattak, and B. Huang. Multivariate Random-Parameters Zero-Inflated Negative Binomial Regression Model: An Application to Estimate Crash Frequencies at Intersections. *Accident Analysis & Prevention*, Vol. 70, 2014, pp. 320–329. <https://doi.org/10.1016/j.aap.2014.04.018>.
- Abdel-Aty, M., and X. Wang. Crash Estimation at Signalized Intersections Along Corridors: Analyzing Spatial Effect and Identifying Significant Factors. *Transportation Research Record: Journal of the Transportation Research Board*, 2006. 1953: 98–111.
- Lee, T., C. Cunningham, and N. Roushail. Movement-Based Intersection Crash Frequency Modeling. *Journal of Transportation Safety & Security*, Vol. 15, No. 5, 2023, pp. 493–514. <https://doi.org/10.1080/19439962.2022.2092571>.
- Park, H.-C., S. Yang, P. Y. Park, and D.-K. Kim. Multiple Membership Multilevel Model to Estimate Intersection Crashes. *Accident Analysis & Prevention*, Vol. 144, 2020, p. 105589. <https://doi.org/10.1016/j.aap.2020.105589>.
- Xie, K., X. Wang, K. Ozbay, and H. Yang. Crash Frequency Modeling for Signalized Intersections in a High-Density Urban Road Network. *Analytic Methods in Accident Research*, Vol. 2, 2014, pp. 39–51. <https://doi.org/10.1016/j.amar.2014.06.001>.
- Huang, H., H. Zhou, J. Wang, F. Chang, and M. Ma. A Multivariate Spatial Model of Crash Frequency by Transportation Modes for Urban Intersections. *Analytic Methods in Accident Research*, Vol. 14, 2017, pp. 10–21. <https://doi.org/10.1016/j.amar.2017.01.001>.
- Chin, H. C., and M. A. Quddus. Applying the Random Effect Negative Binomial Model to Examine Traffic Accident Occurrence at Signalized Intersections. *Accident Analysis & Prevention*, Vol. 35, No. 2, 2003, pp. 253–259. [https://doi.org/10.1016/S0001-4575\(02\)00003-9](https://doi.org/10.1016/S0001-4575(02)00003-9).

17. Xie, K., X. Wang, H. Huang, and X. Chen. Corridor-Level Signalized Intersection Safety Analysis in Shanghai, China Using Bayesian Hierarchical Models. *Accident Analysis & Prevention*, Vol. 50, 2013, pp. 25–33. <https://doi.org/10.1016/j.aap.2012.10.003>.
18. Megat-Johari, M.-U., B. Bazargani, T. J. Kirsch, T. P. Barrette, and P. T. Savolainen. An Examination of the Safety of Signalized Intersections in Consideration of Nearby Access Points. *Transportation Research Record: Journal of the Transportation Research Board*, 2018. 2672: 11–21.
19. Wong, S. C., N. N. Sze, and Y. C. Li. Contributory Factors to Traffic Crashes at Signalized Intersections in Hong Kong. *Accident Analysis & Prevention*, Vol. 39, No. 6, 2007, pp. 1107–1113. <https://doi.org/10.1016/j.aap.2007.02.009>.
20. Li, X., S. Yu, X. Huang, B. Dadashova, W. Cui, and Z. Zhang. Do Underserved and Socially Vulnerable Communities Observe More Crashes? A Spatial Examination of Social Vulnerability and Crash Risks in Texas. *Accident Analysis & Prevention*, Vol. 173, 2022, p. 106721. <https://doi.org/10.1016/j.aap.2022.106721>.
21. Abdel-Aty, M., J. Ugan, and Z. Islam. Exploring the Influence of Drivers' Visual Surroundings on Speeding Behavior. *Accident Analysis & Prevention*, Vol. 198, 2024, p. 107479. <https://doi.org/10.1016/j.aap.2024.107479>.
22. Cai, Q., M. Abdel-Aty, J. Yuan, J. Lee, and Y. Wu. Real-Time Crash Prediction on Expressways Using Deep Generative Models. *Transportation Research Part C: Emerging Technologies*, Vol. 117, 2020, p. 102697. <https://doi.org/10.1016/j.trc.2020.102697>.
23. Stiles, J., Y. Li, and H. J. Miller. How Does Street Space Influence Crash Frequency? An Analysis Using Segmented Street View Imagery. *Environment and Planning B: Urban Analytics and City Science*, Vol. 49, No. 9, 2022, pp. 2467–2483. <https://doi.org/10.1177/23998083221090962>.
24. Kwon, J.-H., and G.-H. Cho. An Examination of the Intersection Environment Associated with Perceived Crash Risk Among School-Aged Children: Using Street-Level Imagery and Computer Vision. *Accident Analysis & Prevention*, Vol. 146, 2020, p. 105716. <https://doi.org/10.1016/j.aap.2020.105716>.
25. Cai, Q., M. Abdel-Aty, O. Zheng, and Y. Wu. Applying Machine Learning and Google Street View to Explore Effects of Drivers' Visual Environment on Traffic Safety. *Transportation Research Part C: Emerging Technologies*, Vol. 135, 2022, p. 103541. <https://doi.org/10.1016/j.trc.2021.103541>.
26. Yue, H. Investigating the Influence of Streetscape Environmental Characteristics on Pedestrian Crashes at Intersections Using Street View Images and Explainable Machine Learning. *Accident Analysis & Prevention*, Vol. 205, 2024, p. 107693. <https://doi.org/10.1016/j.aap.2024.107693>.
27. Dong, C., J. Shi, B. Huang, X. Chen, and Z. Ma. A Study of Factors Affecting Intersection Crash Frequencies Using Random-Parameter Multivariate Zero-Inflated Models. *International Journal of Injury Control and Safety Promotion*, Vol. 24, No. 2, 2017, pp. 208–221. <https://doi.org/10.1080/17457300.2016.1166138>.
28. Nightingale, E., N. Parvin, C. Seiberlich, P. T. Savolainen, and M. Pawlovich. Investigation of Skew Angle and Other Factors Influencing Crash Frequency at High-Speed Rural Intersections. *Transportation Research Record: Journal of the Transportation Research Board*, 2017. 2636: 9–14.
29. Mathew, S., S. S. Pulugurtha, and S. Duvvuri. Exploring the Effect of Road Network, Demographic, and Land Use Characteristics on Teen Crash Frequency Using Geographically Weighted Negative Binomial Regression. *Accident Analysis & Prevention*, Vol. 168, 2022, p. 106615. <https://doi.org/10.1016/j.aap.2022.106615>.
30. Pulugurtha, S. S., and V. R. Sambhara. Pedestrian Crash Estimation Models for Signalized Intersections. *Accident Analysis & Prevention*, Vol. 43, No. 1, 2011, pp. 439–446. <https://doi.org/10.1016/j.aap.2010.09.014>.
31. Patwary, A. L., A. M. Haque, I. Mahdinia, and A. J. Khatak. Investigating Transportation Safety in Disadvantaged Communities by Integrating Crash and Environmental Justice Data. *Accident Analysis & Prevention*, Vol. 194, 2024, p. 107366. <https://doi.org/10.1016/j.aap.2023.107366>.
32. Al-Omari, M. M. A., M. Abdel-Aty, and Q. Cai. Crash Analysis and Development of Safety Performance Functions for Florida Roads in the Framework of the Context Classification System. *Journal of Safety Research*, Vol. 79, 2021, pp. 1–13. <https://doi.org/10.1016/j.jsr.2021.08.004>.
33. Mahmoud, N., M. Abdel-Aty, Q. Cai, and O. Zheng. Vulnerable Road Users' Crash Hotspot Identification on Multi-Lane Arterial Roads Using Estimated Exposure and Considering Context Classification. *Accident Analysis & Prevention*, Vol. 159, 2021, p. 106294. <https://doi.org/10.1016/j.aap.2021.106294>.
34. Yang, J., L. Zhao, J. McBride, and P. Gong. Can You See Green? Assessing the Visibility of Urban Forests in Cities. *Landscape and Urban Planning*, Vol. 91, No. 2, 2009, pp. 97–104. <https://doi.org/10.1016/j.landurbplan.2008.12.004>.
35. Li, X., C. Zhang, W. Li, R. Ricard, Q. Meng, and W. Zhang. Assessing Street-Level Urban Greenery Using Google Street View and a Modified Green View Index. *Urban Forestry & Urban Greening*, Vol. 14, No. 3, 2015, pp. 675–685. <https://doi.org/10.1016/j.ufug.2015.06.006>.
36. Xue, H., P. Guo, Y. Li, and J. Ma. Integrating Visual Factors in Crash Rate Analysis at Intersections: An AutoML and SHAP Approach Towards Cycling Safety. *Accident Analysis & Prevention*, Vol. 200, 2024, p. 107544. <https://doi.org/10.1016/j.aap.2024.107544>.
37. Long, J., E. Shelhamer, and T. Darrell. Fully Convolutional Networks for Semantic Segmentation. *Proc., IEEE Conference on Computer Vision and Pattern Recognition*, Boston, MA, Computer Vision Foundation, June 7–12, 2015, pp. 3431–3440.
38. Dosovitskiy, A., L. Beyer, A. Kolesnikov, D. Weissenborn, X. Zhai, T. Unterthiner, M. Dehghani, et al. An Image Is Worth 16x16 Words: Transformers for Image Recognition at Scale. <http://arxiv.org/abs/2010.11929>. Accessed July 19, 2024.
39. Strudel, R., R. Garcia, I. Laptev, and C. Schmid. Segmenter: Transformer for Semantic Segmentation. *Proc., IEEE/*

- CVF International Conference on Computer Vision*, Computer Vision Foundation, 2021, pp. 7262–7272.
40. Cheng, B., A. G. Schwing, and A. Kirillov. Per-Pixel Classification Is Not All You Need for Semantic Segmentation. <http://arxiv.org/abs/2107.06278>. Accessed November 15, 2024.
 41. Hasan, T., and M. Abdel-Aty. Short-Term Safety Performance Functions by Random Parameters Negative Binomial-Lindley Model for Part-Time Shoulder Use. *Accident Analysis & Prevention*, Vol. 199, 2024, p. 107498. <https://doi.org/10.1016/j.aap.2024.107498>.
 42. Tahir, H. B., S. Yasmin, and M. M. Haque. A Poisson Lognormal-Lindley Model for Simultaneous Estimation of Multiple Crash-Types: Application of Multivariate and Pooled Univariate Models. *Analytic Methods in Accident Research*, Vol. 41, 2024, p. 100315. <https://doi.org/10.1016/j.amar.2023.100315>.
 43. Zamani, H., & Ismail, N. (2010). Negative binomial-Lindley distribution and its application. *Journal of mathematics and statistics*, 6(1), 4–9
 44. Geedipally, S. R., D. Lord, and S. S. Dhavala. The Negative Binomial-Lindley Generalized Linear Model: Characteristics and Application Using Crash Data. *Accident Analysis & Prevention*, Vol. 45, 2012, pp. 258–265. <https://doi.org/10.1016/j.aap.2011.07.012>.
 45. Barua, S., K. El-Basyouny, and M. T. Islam. Multivariate Random Parameters Collision Count Data Models with Spatial Heterogeneity. *Analytic Methods in Accident Research*, Vol. 9, 2016, pp. 1–15. <https://doi.org/10.1016/j.amar.2015.11.002>.
 46. Naznin, F., G. Currie, D. Logan, and M. Sarvi. Application of a Random Effects Negative Binomial Model to Examine Tram-Involved Crash Frequency on Route Sections in Melbourne, Australia. *Accident Analysis & Prevention*, Vol. 92, 2016, pp. 15–21. <https://doi.org/10.1016/j.aap.2016.03.012>.
 47. Lunn, D. J., A. Thomas, N. Best, and D. Spiegelhalter. WinBUGS - A Bayesian Modelling Framework: Concepts, Structure, and Extensibility. *Statistics and Computing*, Vol. 10, No. 4, 2000, pp. 325–337. <https://doi.org/10.1023/A:1008929526011>.
 48. Chen, T., Y. D. Wong, X. Shi, and X. Wang. Optimized Structure Learning of Bayesian Network for Investigating Causation of Vehicles' on-Road Crashes. *Reliability Engineering & System Safety*, Vol. 224, 2022, p. 108527. <https://doi.org/10.1016/j.ress.2022.108527>.
 49. Chen, T., Y. D. Wong, X. Shi, and Y. Yang. A Data-Driven Feature Learning Approach Based on Copula-Bayesian Network and Its Application in Comparative Investigation on Risky Lane-Changing and Car-Following Maneuvers. *Accident Analysis & Prevention*, Vol. 154, 2021, p. 106061. <https://doi.org/10.1016/j.aap.2021.106061>.
 50. Mitra, S., and S. Washington. On the Nature of Over-Dispersion in Motor Vehicle Crash Prediction Models. *Accident Analysis & Prevention*, Vol. 39, No. 3, 2007, pp. 459–468. <https://doi.org/10.1016/j.aap.2006.08.002>.
 51. Gu, Z., I. Bejleri, and B. Peng. Exploring Characteristics and Influencing Factors of Crash Duration on Urban Arterials and Collectors. *Journal of Transportation Safety & Security*, Vol. 14, No. 9, 2022, pp. 1470–1489.
 52. Van Treese, J. W. II, A. K. Koeser, G. E. Fitzpatrick, M. T. Olexa, and E. J. Allen. A Review of the Impact of Roadway Vegetation on Drivers' Health and Well-Being and the Risks Associated with Single-Vehicle Crashes. *Arboricultural Journal*, Vol. 39, No. 3, 2017, pp. 179–193. <https://doi.org/10.1080/03071375.2017.1374591>.
 53. Tice, P. C., S. dey Tirtha, N. Eluru, and P. A. Hancock. Attentiveness in Urban Spaces: The Rhythm of the Street. *Transportation Research Interdisciplinary Perspectives*, Vol. 25, 2024, p. 101063. <https://doi.org/10.1016/j.trip.2024.101063>.
 54. Tice, P. C., P. A. Hancock, S. D. Tirtha, and N. Eluru. The Conditioned Anticipation of People (CAP) Model of Driving in Urban Spaces. *Transportation Research Part F: Traffic Psychology and Behaviour*, Vol. 84, 2022, pp. 301–312. <https://doi.org/10.1016/j.trf.2021.11.012>.
 55. Mahmoudi, J., C. Xiong, M. Yang, and W. Luo. Modeling the Frequency of Pedestrian and Bicyclist Crashes at Intersections: Big Data-Driven Evidence from Maryland. *Transportation Research Record: Journal of the Transportation Research Board*, 2023, 2677: 1245–1260.
 56. Rosencrantz, H., K. Edvardsson, and S. O. Hansson. Vision Zero – Is It Irrational? *Transportation Research Part A: Policy and Practice*, Vol. 41, No. 6, 2007, pp. 559–567. <https://doi.org/10.1016/j.tra.2006.11.002>.
 57. Underwood, G. *Traffic and Transport Psychology: Theory and Application*. Elsevier, Amsterdam, Netherlands, 2005.
 58. Yu, B., Y. Chen, and S. Bao. Quantifying Visual Road Environment to Establish a Speeding Prediction Model: An Examination Using Naturalistic Driving Data. *Accident Analysis & Prevention*, Vol. 129, 2019, pp. 289–298. <https://doi.org/10.1016/j.aap.2019.05.011>.
 59. Noland, R. B., N. J. Klein, and N. K. Tulach. Do Lower Income Areas Have More Pedestrian Casualties? *Accident Analysis & Prevention*, Vol. 59, 2013, pp. 337–345. <https://doi.org/10.1016/j.aap.2013.06.009>.
 60. Wang, X., and M. Abdel-Aty. Temporal and Spatial Analyses of Rear-End Crashes at Signalized Intersections. *Accident Analysis & Prevention*, Vol. 38, No. 6, 2006, pp. 1137–1150. <https://doi.org/10.1016/j.aap.2006.04.022>.
 61. Ambros, J., L. Tomešová, C. Jurewicz, and V. Valentová. A Review of the Best Practice in Traffic Calming Evaluation. *Accident Analysis & Prevention*, Vol. 189, 2023, p. 107073. <https://doi.org/10.1016/j.aap.2023.107073>.
 62. Hu, W., and J. B. Cicchino. The Effects of Left-Turn Traffic-Calming Treatments on Conflicts and Speeds in Washington, DC. *Journal of Safety Research*, Vol. 75, 2020, pp. 233–240. <https://doi.org/10.1016/j.jsr.2020.10.001>.
 63. Wang, C., M. Abdel-Aty, and L. Han. Effects of Speed Difference on Injury Severity of Freeway Rear-End Crashes: Insights from Correlated Joint Random Parameters Bivariate Probit Models and Temporal Instability. *Analytic Methods in Accident Research*, Vol. 42, 2024, p. 100320. <https://doi.org/10.1016/j.amar.2024.100320>.
 64. Han, L., R. Yu, C. Wang, and M. Abdel-Aty. Transformer-Based Modeling of Abnormal Driving Events for

- Freeway Crash Risk Evaluation. *Transportation Research Part C: Emerging Technologies*, Vol. 165, 2024, p. 104727. <https://doi.org/10.1016/j.trc.2024.104727>.
65. Huo, X., J. Leng, Q. Hou, L. Zheng, and L. Zhao. Assessing the Explanatory and Predictive Performance of a Random Parameters Count Model with Heterogeneity in Means and Variances. *Accident Analysis & Prevention*, Vol. 147, 2020, p. 105759. <https://doi.org/10.1016/j.aap.2020.105759>.
66. Wang, W., Y. Yang, X. Yang, V. V. Gayah, Y. Wang, J. Tang, and Z. Yuan. A Negative Binomial Lindley Approach Considering Spatiotemporal Effects for Modeling Traffic Crash Frequency with Excess Zeros. *Accident Analysis & Prevention*, Vol. 207, 2024, p. 107741. <https://doi.org/10.1016/j.aap.2024.107741>.
67. Wang, C., M. Abdel-Aty, and L. Han. Grouped Random Parameters Poisson-Lindley Model with Spatial Effects Addressing Crashes at Intersections: Insights from Visual Environment Features and Spatiotemporal Instability. *Analytic Methods in Accident Research*, Vol. 47, 2025, p. 100387. <https://doi.org/10.1016/j.amar.2025.100387>.